
















Discovery of thionylimide, HNSO, in space: the first N-, S- and O-bearing interstellar molecule

MIGUEL SANZ-NOVO ¹, VÍCTOR M. RIVILLA ¹, HOLGER S. P. MÜLLER ², IZASKUN JIMÉNEZ-SERRA ¹,
JESÚS MARTÍN-PINTADO ¹, LAURA COLZI ¹, SHAOSHAN ZENG ³, ANDRÉS MEGÍAS ¹, ÁLVARO LÓPEZ-GALLIFA ¹,
ANTONIO MARTÍNEZ-HENARES ¹, BELÉN TERCERO ⁴, PABLO DE VICENTE ⁵, DAVID SAN ANDRÉS ¹,
SERGIO MARTÍN ^{6,7} AND MIGUEL A. REQUENA-TORRES ^{8,9}

¹Centro de Astrobiología (CAB), INTA-CSIC, Carretera de Ajalvir km 4, Torrejón de Ardoz, 28850 Madrid, Spain

²I. Physikalisches Institut, Universität zu Köln, Zùlpicher Str. 77, 50937 Köln, Germany

³Star and Planet Formation Laboratory, Cluster for Pioneering Research, RIKEN, 2-1 Hirosawa, Wako, Saitama, 351-0198, Japan

⁴Observatorio Astronómico Nacional (OAN-IGN), Calle Alfonso XII, 3, 28014 Madrid, Spain

⁵Observatorio de Yebes (OY-IGN), Cerro de la Palera SN, Yebes, Guadalajara, Spain

⁶European Southern Observatory, Alonso de Córdova 3107, Vitacura 763 0355, Santiago, Chile

⁷Joint ALMA Observatory, Alonso de Córdova 3107, Vitacura 763 0355, Santiago, Chile

⁸University of Maryland, College Park, ND 20742-2421 (USA)

⁹Department of Physics, Astronomy and Geosciences, Towson University, Towson, MD 21252, USA

ABSTRACT

We present the first detection in space of thionylimide (HNSO) toward the Galactic Center molecular cloud G+0.693-0.027, thanks to the superb sensitivity of an ultradeep molecular line survey carried out with the Yebes 40 m and IRAM 30 m telescopes. This molecule is the first species detected in the interstellar medium containing, simultaneously, N, S and O. We have identified numerous $K_a = 0, 1$ and 2 transitions belonging to HNSO covering from $J_{\text{up}} = 2$ to $J_{\text{up}} = 10$, including several completely unblended features. We derive a molecular column density of $N = (8 \pm 1) \times 10^{13} \text{ cm}^{-2}$, yielding a fractional abundance relative to H_2 of $\sim 6 \times 10^{-10}$, which is about ~ 37 and ~ 4.8 times less abundant than SO and SO_2 , respectively. Although there are still many unknowns in the interstellar chemistry of NSO-bearing molecules, we propose that HNSO is likely formed through the reaction of the NSO radical and atomic H on the surface of icy grains, with alternative routes also deserving exploration. Finally, HNSO appears as a promising link between N-, S- and O- interstellar chemistry and its discovery paves the route to the detection of a new family of molecules in space.

Keywords: Interstellar molecules(849), Interstellar clouds(834), Galactic center(565), Spectral line identification(2073), Astrochemistry(75)

1. INTRODUCTION

In recent years, astrochemistry has witnessed an outburst of new interstellar detections, with more than 75 new species discovered since 2021.¹ These species contain the six chemical elements essential for life: carbon (C), hydrogen (H), oxygen (O), nitrogen (N), phosphorus (P), and sulfur (S); and many of them are considered molecular precursors of prebiotic chemistry (e.g. Belloche et al. 2008; Belloche et al. 2019; Zeng et al. 2019; Rivilla et al. 2019, 2021a, 2022; Jiménez-Serra et al. 2022). However, despite the plethora of new species, NSO compounds (i.e., molecules containing simultane-

ously N, S and O) have attracted little attention from the astronomical community, although they appear as a promising yet unexplored link between the chemistry of N-, S- and O-bearing species in the ISM.

On Earth, the NSO chemistry plays a key biological role in transmitting signals both within and between cells and tissues (Foster et al. 2009; Miljkovic et al. 2013). In particular, several [H,N,S,O] isomers (e.g. HSNO, HONS and HNSO) are thought to connect the biochemistries of two important biological messengers, nitric oxide (NO) and hydrogen sulfide (H_2S) (Filipovic et al. 2012; Miljkovic et al. 2013; Ivanova et al. 2014; Nava et al. 2016; Kumar & Francisco 2017). NO, as the first gasotransmitter, is involved in the regulation of vascular tone and heart function, among other physiological

¹ <https://cdms.astro.uni-koeln.de/classic/molecules>

processes (Wu et al. 2018). Meanwhile, H₂S plays a positive role regarding antioxidative stress and inflammation regulation (Zhao et al. 2024). NSO-bearing compounds are also very abundant in oil sands (Ji et al. 2021) and contain rich geological and geochemical data (Shi et al. 2010; Noah et al. 2015; Ziegs et al. 2018; Chang et al. 2023), excelling in recording biotic and palaeoenvironmental signatures (Yue 2023), and thus are of interest for astrobiology.

This fact triggered us to explore the chemistry of NSO compounds in the ISM. As a proof of concept, we targeted the study of thionylimide, HNSO, which can be seen as an NH- analogue of sulfur dioxide, SO₂, where one O atom of O=S=O is replaced by a NH- group, yielding HN=S=O. This molecule has been suggested to be the parent species of interstellar NS (Barbier et al. 2006), and appears as a promising candidate since both SO and SO₂ are particularly abundant in the ISM (Snyder et al. 1975; Cernicharo et al. 2011; Vidal et al. 2017). However, despite its experimental microwave characterization being performed long ago (Kirchhoff 1969; Borgo et al. 1979; Heineking & Gerry 1993), to our knowledge, HNSO has only been searched for toward Orion KL yielding no detection (Esplugues et al. 2013).

In this letter, we report the discovery in space of HNSO, the first interstellar N-, S- and O-bearing molecule, toward the Galactic center (GC) molecular cloud G+0.693-0.027 (hereafter G+0.693). We selected G+0.693 to conduct the astronomical search since it is rich in O-bearing (Requena-Torres et al. 2006; Rivilla et al. 2022; Jiménez-Serra et al. 2022; Sanz-Novo et al. 2023), S-bearing (Rodríguez-Almeida et al. 2021; Sanz-Novo et al. 2024), and N-bearing species (Zeng et al. 2018; Rivilla et al. 2019, 2021b; Jiménez-Serra et al. 2020; Zeng et al. 2021), of which some contain also oxygen (Rivilla et al. 2020, 2021a, 2023; Zeng et al. 2023).

2. OBSERVATIONS

We have analyzed data from an unbiased ultradeep spectral survey conducted toward the GC molecular cloud G+0.693. We covered the Q-band (31.075-50.424 GHz) using the Yebes 40 m (Guadalajara, Spain) radiotelescope. Also, we covered three additional frequency windows with high sensitivity using the IRAM 30 m (Granada, Spain) radiotelescope: 83.2–115.41 GHz, 132.28–140.39 and 142.00–173.81 GHz. For these observations, we used the position switching mode, centered at $\alpha = 17^{\text{h}}47^{\text{m}}22^{\text{s}}$, $\delta = -28^{\circ}21'27''$, with the off position shifted by $\Delta\alpha = -885''$ and $\Delta\delta = 290''$. The half power beam width (HPBW) of the Yebes 40 m telescope varies between $\sim 35''$ - $55''$ (at 50 and 31 GHz, respectively; Tercero et al. 2021) and the HPBW of the

IRAM 30 m radiotelescope is $\sim 14''$ – $29''$ across the frequency range covered. Also, we assumed that the molecular emission toward G+0.693 is extended as compared to the telescope beam (Jones et al. 2012; Li et al. 2020; Zheng et al. 2024). More details of these observations (e.g., resolution and noise levels of the spectral survey) were provided in Rivilla et al. (2023) and Sanz-Novo et al. (2023).

3. DETECTION OF HNSO

HNSO may occur in the *cis*- and in the *trans*-configuration, but only the former (hereafter HNSO) has been detected experimentally in the laboratory. It is an asymmetric rotor close to the prolate symmetric limit with $\kappa = (2B - A - C)/(A - C) = -0.9190$, and possesses a sizable *a*-dipole moment component of 0.893 D and a much weaker *b*-component of 0.181 D. It was firstly characterized by microwave spectroscopy more than fifty years ago by Kirchhoff (1969). The astronomical line identification of HNSO has been performed using entry 63514 of the Cologne Database for Molecular Spectroscopy (CDMS²; Müller et al. 2005; Endres et al. 2016), explained in detail in Appendix A, which has been implemented into the MADCUBA package (Martín et al. 2019). We did not consider the hyperfine structure, since it is not resolved owing to the typical broad linewidths of the molecular line emission measured toward G+0.693 (FWHM ~ 15 – 20 km s⁻¹; Requena-Torres et al. 2006, 2008; Zeng et al. 2018; Rivilla et al. 2022c).

We used the Spectral Line Identification and Modeling (SLIM) tool (version from 2023, November 15) within MADCUBA, which, assuming a Local Thermodynamic Equilibrium (LTE) excitation condition, enables the creation of LTE synthetic spectra to be subsequently compared with the observed astronomical data. After evaluating the emission of more than 130 molecules previously identified toward G+0.693, we managed to detect numerous $K_a = 0, 1$ and 2 transitions spanning from $J_{\text{up}} = 2$ to $J_{\text{up}} = 10$. The most intense unblended or slightly blended features are shown in Figure 1, and their spectroscopic information is listed in Table 1. Among them, we found six completely unblended transitions. Other transitions reproduce well the observations, once the blending with emission from other molecules previously detected toward G+0.693 is considered (see Figure 1 and Table 1). The remaining lines, blended with more prominent transitions from other species, are also in agreement with the observed spectra.

² <https://cdms.astro.uni-koeln.de/classic/entries/archive/HNSO/>

Table 1. Spectroscopic information of the unblended or slightly blended transitions of HNSO detected toward G+0.693–0.027 (shown in Figure 1).

Frequency (GHz)	Transition ^(a)	log I (300 K) (nm ² MHz)	E_{up} (K)	rms (mK)	$\int T_{\text{A}}^* dv$ (mK km s ⁻¹)	S/N ^(b)	Blending
34.4854073 (9)	2 _{1,2} –1 _{1,1}	–6.1721	4.4	0.5	166	60	U-line
71.7851541 (19)	4 _{0,4} –3 _{0,3}	–5.1148	8.6	2.4	829	60	HOCH ₂ CN
75.5211379 (19)	4 _{1,3} –3 _{1,2}	–5.1015	10.9	1.8	745	72	CH ₃ CHO
85.9961329 (25)	5 _{1,4} –4 _{1,4}	–4.8860	14.2	1.1	342	54	Unblended*
89.3545678 (25)	5 _{0,5} –4 _{0,4}	–4.8337	12.8	1.0	477	83	Unblended*
91.2765634 (25)	5 _{2,3} –4 _{2,2}	–4.9013	20.7	1.1	547	87	¹⁸ OCS
94.2963295 (25)	5 _{1,4} –4 _{1,3}	–4.8074	15.4	1.0	393	69	Unblended*
106.6915343 (32)	6 _{0,6} –5 _{0,5}	–4.6077	17.9	1.4	595	74	Unblended*
109.9674387 (37)	6 _{2,4} –5 _{2,3}	–4.6427	25.9	1.6	252	27	U-line
112.9958897 (33)	6 _{1,5} –5 _{1,4}	–4.5729	20.8	1.6	364	40	Unblended*
131.5991163 (43)	7 _{1,6} –6 _{1,5}	–4.3789	27.1	5.4	613	20	C ₂ H ₅ CHO
137.0214017 (58)	8 _{1,8} –7 _{1,7}	–4.2898	31.4	1.1	278	44	N-CH ₃ NHCHO
140.6185667 (57)	8 _{0,8} –7 _{0,7}	–4.2610	30.5	1.3	419	56	U-line
143.9633403 (59)	8 _{2,7} –7 _{2,6}	–4.2782	38.6	1.3	180	24	Unblended*
147.9246044 (60)	8 _{2,6} –7 _{2,5}	–4.2550	39.1	1.0	313	55	HC ₂ CHO
150.0824046 (57)	8 _{1,7} –7 _{1,6}	–4.2146	34.2	1.1	209	33	CH ₃ ¹³ CHO
168.4191360 (74)	9 _{1,8} –8 _{1,7}	–4.0732	42.3	1.6	172	19	H ₂ COH ⁺ , OCS
170.711716 (10)	10 _{1,10} –9 _{1,9}	–4.0210	46.9	1.0	150	26	HCS ⁺

NOTE—^(a) The rotational energy levels are labelled using the conventional notation for asymmetric tops: J_{K_a, K_c} , where J denotes the angular momentum quantum number, and the K_a and K_c labels are projections of J along the a and c principal axes. ^(b) The S/N ratio is computed from the integrated signal ($\int T_{\text{A}}^* dv$) and noise level, $\sigma = \text{rms} \times \sqrt{\delta v \times \text{FWHM}}$, where δv is the velocity resolution of the spectra and the FWHM is fitted from the data. Numbers in parentheses represent the predicted uncertainty associated to the last digits.

The “*” symbol designates those transitions used in the initial fit. We denote as U-line the line blending with a yet unidentified feature.

The best LTE modelling for HNSO was achieved using a two-step approach as described in San Andrés et al. (submitted, 2024). The line width (FWHM) was constrained first using exclusively the aforementioned unblended transitions (marked with a “*” symbol in Table 1), obtaining a value of $\text{FWHM} = 21.5 \pm 0.6 \text{ km s}^{-1}$ in an initial nonlinear least-squares LTE fit using the AUTOFIT tool within SLIM (Martín et al. 2019). Afterward, we performed a second fit that includes all the transitions shown in Figure 1 and Table 1, with the exception of the 8_{0,8}–7_{0,7} (slightly contaminated with an unidentified line), fixing the line width and leaving as free parameters the excitation temperature, T_{ex} , radial velocity, v_{LSR} , and column density, N . We derived a molecular column density of $N(\text{HNSO}) = (8 \pm 1) \times 10^{13} \text{ cm}^{-2}$, which yields a fractional abundance with respect to molecular hydrogen of $(6 \pm 1) \times 10^{-10}$, using $N(\text{H}_2) = 1.35 \times 10^{23} \text{ cm}^{-2}$ as derived by Martín et al. (2008) employing C¹⁸O as a total H₂ column density tracer and assuming a C¹⁸O/H₂ abundance ratio of 1.7×10^7 , Frerking et al. (1982)). Additionally, we obtained a $T_{\text{ex}} = 11$

$\pm 2 \text{ K}$ and a $v_{\text{LSR}} = 68 \pm 2 \text{ km s}^{-1}$, which are consistent with those found for other molecular species toward the same source (see e.g. Requena-Torres et al. 2006; Zeng et al. 2018). As shown in Table 1, the detected transitions cover a wide range of E_{up} , which allowed us to derive an accurate estimate on the T_{ex} . The fitted line profiles of HNSO are shown using a red line in Figure 1 overlaid with the observed spectra (in gray). In blue, we report the predicted spectrum considering all molecular species identified and analyzed toward G+0.693.

We have also performed a complementary rotational diagram analysis (Goldsmith & Langer 1999), as implemented in MADCUBA, using transitions that are unblended with the emission from other molecules, together with the 8_{1,7}–7_{1,6} transition (at 150.0824046 GHz) which is negligibly contaminated by the emission of CH₃¹³CHO, and considering the velocity-integrated intensity over the line width (Rivilla et al. 2021a). We obtained the following physical parameters for HNSO: $N = (7.0 \pm 0.8) \times 10^{13} \text{ cm}^{-2}$ and $T_{\text{ex}} = 11.9 \pm 0.6 \text{ K}$, which agree well with those derived from the AUT-

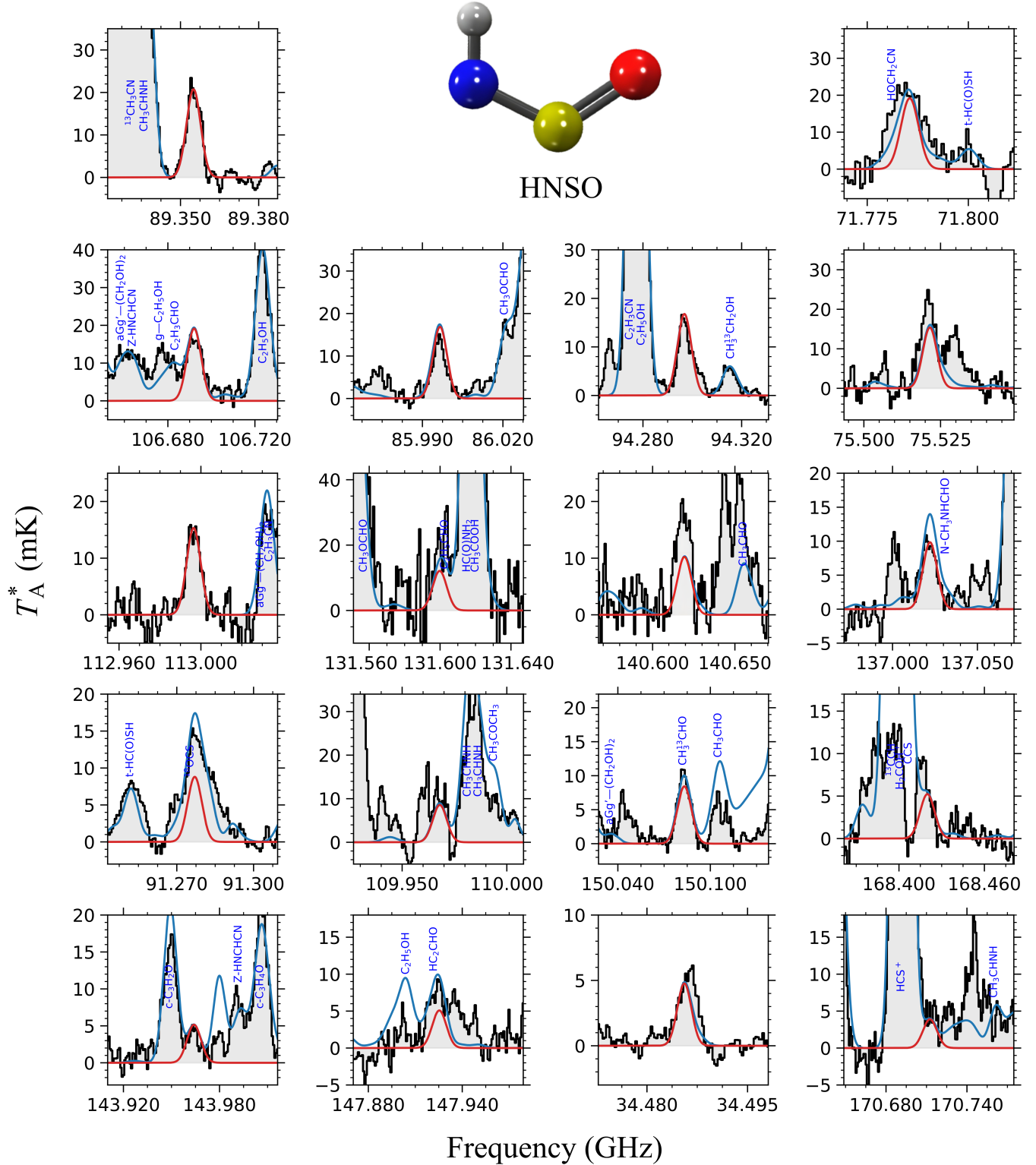


Figure 1. Transitions of HNSO identified toward the GC molecular cloud G+0.693–0.027 (listed in Table 1) sorted by decreasing peak intensity. The result of the best LTE fit of HNSO is plotted with a red line and the blue line depicts the emission from all the molecules identified to date in our survey, including HNSO (observed spectra shown as gray histograms). The structure of HNSO is also shown (nitrogen atom in blue; oxygen atom in red, sulfur atom in yellow and hydrogen atom in white).

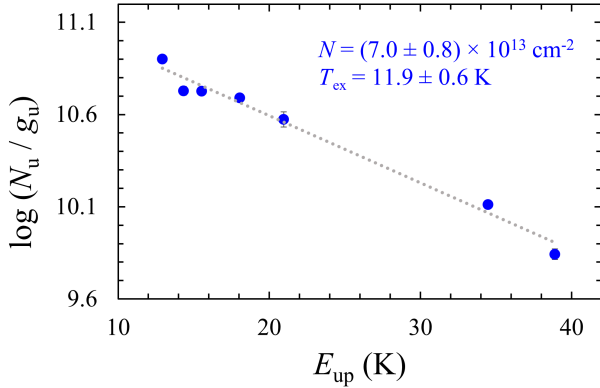


Figure 2. Rotational diagram of HNSO toward G+0.693 (blue dots, including 1σ errors). The best linear fit to the data points is depicted using a gray dotted line. The derived values for the molecular column density, N , and the excitation temperature, T_{ex} , are shown in blue.

OFIT. The results of the analysis are depicted in Figure 2.

4. DISCUSSION

To understand how HNSO fits in a broader astrochemical context, we can compare its abundance with that reported for plausible precursors, such as SO (Rivilla et al. 2022b) and NS (the analysis is detailed in Appendix B), as well as other structurally related molecules also detected toward G+0.693 (see Table 2) highlighting SO_2 (analyzed in Appendix C), HNCS (Sanz-Novo et al. 2024), HNSO (Zeng et al. 2018) and HOCN (Rivilla et al. 2022c). We found a $N(\text{SO})/N(\text{HNSO})$ ratio of 37 ± 4 toward G+0.693, which is significantly lower than the lower limit ratio derived toward Orion KL ($N(\text{SO})/N(\text{HNSO}) \geq 2600$; Esplugues et al. 2013). Moreover, we obtained a $N(\text{SO}_2)/N(\text{HNSO})$ ratio of 4.8 ± 0.6 , a $N(\text{HNCS})/N(\text{HNSO})$ ratio of 0.8 ± 0.1 , a $N(\text{HNSO})/N(\text{HNSO})$ ratio of 40 ± 6 and a $N(\text{HOCN})/N(\text{HNSO})$ ratio of 0.27 ± 0.4 . Consequently, HNSO appears to be a rather abundant molecule within interstellar S-chemistry, despite having gone unnoticed until now. Our observations are in line with the results presented in Sanz-Novo et al. (2024) for a variety of well-known interstellar S-bearing molecules, which suggest that S is not significantly depleted toward G+0.693 compared to other astronomical sources (Martín-Doménech et al. 2016; Vidal et al. 2017; Marcelino et al. 2023; Fuente et al. 2023).

Although HNSO could be a link between N-, S- and O- interstellar chemistry, this species is missing in commonly-used chemical networks, such as the Kinetic Database for Astrochemistry (KIDA; <http://kida.astrophy.u-bordeaux.fr/>) or in the UMIST Database for Astrochemistry (UDfA; Millar et al. 2024). Therefore,

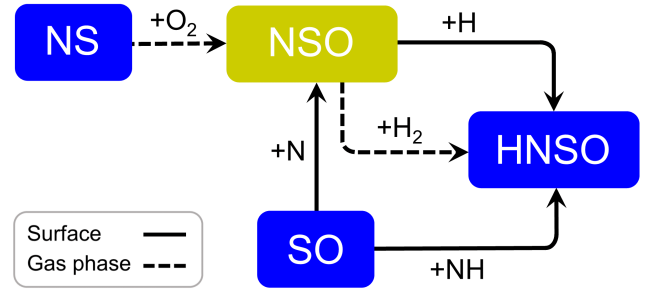


Figure 3. Suggested chemical routes for the formation of HNSO in the ISM. We show in blue molecules that have been identified toward G+0.693 and in yellow molecules that have not been searched for toward G+0.693 because spectroscopy is not available (NSO). Surface reactions are shown in black solid lines while gas-phase reactions are depicted with dashed arrows.

further effort is required to account for the formation of NSO-compounds, which will contribute to achieve a better agreement between observations and chemical models of S-, N- and O-bearing species.

Concerning its production in the ISM, HNSO is most likely formed through the grain-surface reaction between the NSO radical –whose rotational signatures remain unknown and, therefore, it has not been searched for in the ISM so far– and atomic hydrogen. This hydrogenation process is feasible at the dust temperatures measured in the Galactic Center (~ 20 K; Rodríguez-Fernández et al. 2000; Etxaluze et al. 2013). Once HNSO is formed on the grains, it can be subsequently transferred to the gas phase thanks to shock-induced desorption. Alternatively, if we assume a similar grain-surface formation pathway as that explored for HNSO by Quénard et al. (2018), i.e., $\text{NH} + \text{CO} \rightarrow \text{HNSO}$ (Fedoseev et al. 2016), we can propose the following alternative radical-radical diffusion reaction: $\text{NH} + \text{SO} \rightarrow \text{HNSO}$. Note, however, that the diffusion of radicals on grain surfaces is not expected to occur efficiently at temperatures below 30 K (Garrod et al. 2008; Garrod 2013), and thus this mechanism is not expected to be dominant at the low dust temperatures measured in the Galactic Center. Nonetheless, as recently shown in the models of Garrod et al. (2022), non-diffusive chemistry could alternatively yield significant amounts of HNSO even at low dust temperatures via the reaction $\text{NH} + \text{CO} \rightarrow \text{HNSO}$, which suggests that the same could apply to the reaction $\text{NH} + \text{SO} \rightarrow \text{HNSO}$.

In the gas phase, the hydrogenation process has been explored theoretically using high-level coupled cluster methodologies for all possible NSO radical isomers (Kumar & Francisco 2017), suggesting that the formation of their corresponding $[\text{H}, \text{N}, \text{S}, \text{O}]$ hydrides (i.e., HNSO,

Table 2. Derived physical parameters for relevant N-, S- and/or O-bearing molecules related to HNSO detected toward G+0.693-0.027.

Molecule	Formula	N ($\times 10^{14} \text{ cm}^{-2}$)	T_{ex} (K)	v_{LSR} (km s^{-1})	FWHM (km s^{-1})	Abundance ^a ($\times 10^{-10}$)	Ref. ^b
Thionylimide	HNSO	0.8 ± 0.1	11 ± 2	68 ± 2	21.5^c	6 ± 1	(1)
Sulfur monoxide (^{18}O isotopologue)	S^{18}O	0.120 ± 0.003	6.9^c	67.9 ± 0.3	24.8 ± 0.7	0.089 ± 0.008	(2)
Sulfur monoxide	SO	30.06 ± 0.07^d	-	-	-	224 ± 20	(2)
Sulfur dioxide	SO_2	3.84 ± 0.05	18.9 ± 0.2	68.9 ± 0.1	21.1 ± 0.3	28 ± 3	(1)
Nitrogen sulfide	NS	2.8 ± 0.3	7.5 ± 0.5	70.6 ± 0.6	19 ± 1	21 ± 2	(1)
Isothiocyanic acid	HNCS	0.62 ± 0.01	20.4 ± 0.5	66.7 ± 0.3	21.0^c	4.6 ± 0.4	(3)
Isocyanic acid ($K_a = 0$)	HNCO	32 ± 1	17 ± 1	67 ± 1	23 ± 1	239 ± 21	(4)
Cyanic acid	HOCN	0.213 ± 0.004	7.4 ± 0.2	68 ± 0.2	19.2 ± 0.3	0.16 ± 0.01	(5)

NOTE—^a We adopted $N_{\text{H}_2} = 1.35 \times 10^{23} \text{ cm}^{-2}$, from Martín et al. (2008), assuming an uncertainty of 15% of its value. ^b References: (1) This work; (2) Rivilla et al. (2022b); (3) Sanz-Novo et al. (2024); (4) Zeng et al. (2018); (5) Rivilla et al. (2022c). ^c Value fixed in the fit. ^d Computed using the most optically thin isotopologue S^{18}O and assuming a $^{16}\text{O}/^{18}\text{O} = 250$ in the CMZ (Wilson & Rood 1994).

HSNO and SNOH) is exothermic and barrierless, being thus feasible under interstellar conditions. Nevertheless, these authors showed that, once formed, these hydrides will likely decompose yielding SH and NO, SN and OH or SO and NH radicals. Another possible gas-phase route is the reaction between NSO and H_2 , yielding $\text{HNSO} + \text{H}$, which, to the best of our knowledge, remains unexplored.

On the other hand, the formation of the NSO radical, a mixed oxide of nitrogen and sulfur, and also the most stable member of the [N,S,O] isomeric family (Kumar & Francisco 2017), remains uncharted as well. On grains, a possible diffusion mechanism of atomic N on the dust-grain surface cannot be a priori discarded, which, if efficient enough at the typical low temperatures of the icy grain mantles, could react with SO yielding NSO. In this context, it has recently been shown that the diffusion of atomic C is feasible at temperatures above 22 K on icy grain surfaces (Tsuge et al. 2023), which is on the order of the dust temperature of the Galactic Center. Consequently, it would be interesting to extend this investigation on plausible N-insertion reactions driven by the diffusion of N atoms on interstellar ices. Conversely, non-diffusive grain-surface reactions between N and SO may also play a role if they are formed *in situ* (Garrod et al. 2022) (e.g., through early photochemistry within the ices), subsequently yielding NSO. On a similar note, the reaction $\text{N}(\text{gas}) + \text{SO}(\text{grain})$ forming NSO on the grain surface could also be studied, since C-atom addition reactions between C coming from gas-phase and grain-surface species are proved to be efficient (Fedoseev et al. 2022).

In addition, we propose the following gas-phase reaction: $\text{NS} + \text{O}_2 \rightarrow \text{NSO} + \text{O}$, similarly to the NCO

radical, which is produced via $\text{CN} + \text{O}_2 \rightarrow \text{NCO} + \text{O}$ (reaction rate of $2.4 \times 10^{-11} \text{ cm}^{-3} \text{ s}^{-1}$; Glarborg et al. 1998; Marcelino et al. 2018), given that NS is also detected toward G+0.693 (see Appendix B). We find a molecular column density of $N(\text{NS}) = (2.8 \pm 0.3) \times 10^{14} \text{ cm}^{-2}$, which indicates that it is ~ 3.5 times more abundant than HNSO, suggesting that the route starting with NS as plausible precursor may be relevant only if most of the reservoir of NS was locked up in the formation of HNSO. Nonetheless, in this case the NSO radical would need to be subsequently depleted in order to react with atomic H on the ice. All in all, NSO appears as a promising molecule to be studied by the laboratory spectroscopic community.

The feasibility of all the aforementioned routes also needs to be further explored, both theoretically and in the laboratory, to provide conclusive clues on the formation pathways of HNSO. Particularly, the spectroscopic study of other [H,N,S,O] isomers, highlighting the *trans*- form of HNSO, certainly merits attention, given that several stereoisomers³ have been detected toward G+0.693 (e.g., *cis*- and *trans*-formic acid, HCOOH, and the high-energy *cis*-conformer of carbonic acid, HOCOOH; Sanz-Novo et al. 2023).

The results presented in this letter confirm that G+0.693 is an astrochemical niche for the detection of new S-bearing species, even combined with O and/or N. This fact opens the door for the investigation of a new family of interstellar molecules. Moreover, the discovery of the first interstellar NSO-bearing species shall help in

³ Isomers that possess identical constitution, but differ in the three-dimensional orientations of their atoms.

the identification of hitherto unidentified organo-sulfur molecules in the gas phase, pushing also the frontiers of known chemical complexity in the ISM and its possible contribution to prebiotic chemistry.

Software: 1) Madrid Data Cube Analysis (MADCUBA) on ImageJ is a software developed at the Center of Astrobiology (CAB) in Madrid; <https://cab.inta-csic.es/madcuba/>; Martín et al. (2019); version from 2023 November 15.

We are grateful to the IRAM 30 m and Yebes 40 m telescopes staff for their help during the different observing runs, highlighting project 21A014 (PI: Rivilla), project 018-19 (PI: Rivilla) and project 123-22 (PI: Jiménez-Serra). The 40 m radio telescope at Yebes Observatory is operated by the Spanish Geographic Institute (IGN, Ministerio de Transportes, Movilidad y Agenda Urbana). IRAM is supported by INSU/CNRS (France), MPG (Germany) and IGN (Spain). M. S. N. acknowledges a Juan de la Cierva Postdoctoral Fellow project JDC2022-048934-I, funded by the Spanish Ministry of Science, Innovation and Universities/State Agency of Research MICIU/AEI/10.13039/501100011033 and by the European Union "NextGenerationEU"/PRTR". V. M. R. acknowledges support from project number RYC2020-029387-I funded by MCIN/AEI/10.13039/501100011033 and by "ESF, Investing in your future", and from the Consejo Superior de Investigaciones Científicas (CSIC) and the Centro de Astrobiología (CAB) through the project 20225AT015 (Proyectos intramurales especiales del CSIC).. I. J.-S., J. M. -P., L. C, A. M., and A. M. H. acknowledge funding from grants No. PID2019-105552RB-C41 and PID2022-136814NB-I00 from MICIU/AEI/10.13039/501100011033 and by "ERDF A way of making Europe". A. M. has received support from grant PRE2019-091471, funded by MICIU/AEI/10.13039/501100011033 and by "ESF, Investing in your future". A. M. H. acknowledges funds from Grant MDM-2017-0737 Unidad de Excelencia "María de Maeztu" Centro de Astrobiología (CAB, INTA-CSIC). DSA also extends his gratitude for the financial support provided by the Comunidad de Madrid through the Grant PIPF-2022/TEC-25475. P. dV. and B. T. thank the support from MICIU through project PID2019-107115GB-C21. B. T. also thanks the Spanish MICIU for funding support from grant PID2022-137980NB-I00. H. S. P. M. thanks Evan Robertson and Don McNaughton for providing the infrared GSCDs. He also acknowledges support by the Deutsche Forschungsgemeinschaft (DFG) through the collaborative research grant SFB 1601 (project ID 500700252), subprojects Inf and A4. S. Z. acknowledge the support by RIKEN Special Postdoctoral Researchers Program.

REFERENCES

- Barbier, B., Gargaud, M., de Duve, C., Martin, H., & Reisse, J. 2006, Lectures in Astrobiology: Vol I : Part 1: The Early Earth and Other Cosmic Habitats for Life, Study Edition, Advances in Astrobiology and Biogeophysics (Springer Berlin Heidelberg), doi: [10.1007/b10889](https://doi.org/10.1007/b10889)
- Becke, A. D. 1993, JChPh, 98, 5648, doi: [10.1063/1.464913](https://doi.org/10.1063/1.464913)
- Belloche, A., Garrod, R. T., Müller, H. S. P., et al. 2019, A&A, 628, A10, doi: [10.1051/0004-6361/201935428](https://doi.org/10.1051/0004-6361/201935428)

- Belloche, A., Menten, K. M., Comito, C., et al. 2008, *A&A*, 482, 179, doi: [10.1051/0004-6361:20079203](https://doi.org/10.1051/0004-6361:20079203)
- Borgo, A. D., Lonardo, G., Scappini, F., & Trombetti, A. 1979, *Chem. Phys. Lett.*, 63, 115, doi: [10.1016/0009-2614\(79\)80470-4](https://doi.org/10.1016/0009-2614(79)80470-4)
- Cernicharo, J., Agúndez, M., Kahane, C., et al. 2011, *A&A*, 529, L3, doi: [10.1051/0004-6361/201116717](https://doi.org/10.1051/0004-6361/201116717)
- Chang, X., Liu, T., Shi, B., et al. 2023, *Energy Reports*, 9, 1077, doi: <https://doi.org/10.1016/j.egy.2022.12.015>
- Dunning, Jr., T. H. 1989, *J. Chem. Phys.*, 90, 1007, doi: [10.1063/1.456153](https://doi.org/10.1063/1.456153)
- Endres, C. P., Schlemmer, S., Schilke, P., Stutzki, J., & Müller, H. S. P. 2016, *Journal of Molecular Spectroscopy*, 327, 95, doi: [10.1016/j.jms.2016.03.005](https://doi.org/10.1016/j.jms.2016.03.005)
- Esplugues, G. B., Cernicharo, J., Viti, S., et al. 2013, *A&A*, 559, A51, doi: [10.1051/0004-6361/201322073](https://doi.org/10.1051/0004-6361/201322073)
- Etzaluze, M., Goicoechea, J. R., Cernicharo, J., et al. 2013, *A&A*, 556, A137, doi: [10.1051/0004-6361/201321258](https://doi.org/10.1051/0004-6361/201321258)
- Fedoseev, G., Chuang, K. J., van Dishoeck, E. F., Ioppolo, S., & Linnartz, H. 2016, *MNRAS*, 460, 4297, doi: [10.1093/mnras/stw1028](https://doi.org/10.1093/mnras/stw1028)
- Fedoseev, G., Qasim, D., Chuang, K.-J., et al. 2022, *ApJ*, 924, 110, doi: [10.3847/1538-4357/ac3834](https://doi.org/10.3847/1538-4357/ac3834)
- Filipovic, M. R., Miljkovic, J. L., Nauser, T., et al. 2012, *JACS*, 134, 12016, doi: [10.1021/ja3009693](https://doi.org/10.1021/ja3009693)
- Foster, M. W., Hess, D. T., & Stamler, J. S. 2009, *Trends in Molecular Medicine*, 15, 391, doi: <https://doi.org/10.1016/j.molmed.2009.06.007>
- Frerking, M. A., Langer, W. D., & Wilson, R. W. 1982, *The ApJ*, 262, 590, doi: [10.1086/160451](https://doi.org/10.1086/160451)
- Frisch, M. J., Trucks, G. W., Schlegel, H. B., et al. 2019
- Fuente, A., Rivière-Marichalar, P., Beitia-Antero, L., et al. 2023, *A&A*, 670, A114, doi: [10.1051/0004-6361/202244843](https://doi.org/10.1051/0004-6361/202244843)
- Garrod, R. T. 2013, *ApJ*, 765, 60, doi: [10.1088/0004-637X/765/1/60](https://doi.org/10.1088/0004-637X/765/1/60)
- Garrod, R. T., Jin, M., Matis, K. A., et al. 2022, *ApJS*, 259, 1, doi: [10.3847/1538-4365/ac3131](https://doi.org/10.3847/1538-4365/ac3131)
- Garrod, R. T., Weaver, S. L. W., & Herbst, E. 2008, *ApJ*, 682, 283
- Glarborg, P., Alzueta, M. U., Dam-Johansen, K., & Miller, J. A. 1998, *Combustion and Flame*, 115, 1, doi: [https://doi.org/10.1016/S0010-2180\(97\)00359-3](https://doi.org/10.1016/S0010-2180(97)00359-3)
- Goldsmith, P. F., & Langer, W. D. 1999, *ApJ*, 517, 209
- Heineking, N., & Gerry, M. C. L. 1993, *J. Mol. Spectrosc.*, 158, 62, doi: [10.1006/jmsp.1993.1054](https://doi.org/10.1006/jmsp.1993.1054)
- Ivanova, L. V., Anton, B. J., & Timerghazin, Q. K. 2014, *Phys. Chem. Chem. Phys.*, 16, 8476, doi: [10.1039/C4CP00469H](https://doi.org/10.1039/C4CP00469H)
- Ji, H., Li, S., Zhang, H., et al. 2021, *ACS Omega*, 6, 25680, doi: [10.1021/acsomega.1c03801](https://doi.org/10.1021/acsomega.1c03801)
- Jiménez-Serra, I., Martín-Pintado, J., Rivilla, V. M., et al. 2020, *Astrobiology*, 20, 1048
- Jiménez-Serra, I., Rodríguez-Almeida, L. F., Martín-Pintado, J., et al. 2022, *A&A*, 663, A181, doi: [10.1051/0004-6361/202142699](https://doi.org/10.1051/0004-6361/202142699)
- Jones, P. A., Burton, M. G., Cunningham, M. R., et al. 2012, *MNRAS*, 419, 2961, doi: [10.1111/j.1365-2966.2011.19941.x](https://doi.org/10.1111/j.1365-2966.2011.19941.x)
- Joo, D.-L., & Clouthier, D. J. 1996, *J. Chem. Phys.*, 104, 8852, doi: [10.1063/1.471619](https://doi.org/10.1063/1.471619)
- Joo, D.-L., Harjanto, H., & Clouthier, D. J. 1996, *J. Mol. Spectrosc.*, 178, 78, doi: [10.1006/jmsp.1996.0159](https://doi.org/10.1006/jmsp.1996.0159)
- Kirchhoff, W. H. 1969, *J. Am. Chem. Soc.*, 91, 2437, doi: [10.1021/ja01038a006](https://doi.org/10.1021/ja01038a006)
- Kumar, M., & Francisco, J. S. 2017, *The Journal of Physical Chemistry A*, 121, 6652, doi: [10.1021/acs.jpca.7b06344](https://doi.org/10.1021/acs.jpca.7b06344)
- Lee, C., Yang, W., & Parr, R. G. 1988, *PhRvB*, 37, 785, doi: [10.1103/PhysRevB.37.785](https://doi.org/10.1103/PhysRevB.37.785)
- Lee, S. K., Ozeki, H., & Saito, S. 1995, *ApJS*, 98, 351, doi: [10.1086/192165](https://doi.org/10.1086/192165)
- Li, J., Wang, J., Qiao, H., et al. 2020, *MNRAS*, 492, 556, doi: [10.1093/mnras/stz3337](https://doi.org/10.1093/mnras/stz3337)
- Marcelino, N., Agúndez, M., Cernicharo, J., Roueff, E., & Tafalla, M. 2018, *A&A*, 612, L10, doi: [10.1051/0004-6361/201833074](https://doi.org/10.1051/0004-6361/201833074)
- Marcelino, N., Puzzarini, C., Agúndez, M., et al. 2023, *A&A*, 674, L13, doi: [10.1051/0004-6361/202346935](https://doi.org/10.1051/0004-6361/202346935)
- Martín, S., Martín-Pintado, J., Blanco-Sánchez, C., et al. 2019, *A&A*, 631, A159
- Martín, S., Requena-Torres, M. A., Martín-Pintado, J., & Mauersberger, R. 2008, *The ApJ*, 678, 245
- Martín-Doménech, R., Jiménez-Serra, I., Muñoz Caro, G. M., et al. 2016, *A&A*, 585, A112, doi: [10.1051/0004-6361/201526271](https://doi.org/10.1051/0004-6361/201526271)
- Miljkovic, J. L., Kenkel, I., Ivanović-Burmazović, I., & Filipovic, M. R. 2013, *Angewandte Chemie International Edition*, 52, 12061, doi: <https://doi.org/10.1002/anie.201305669>
- Millar, T. J., Walsh, C., Van de Sande, M., & Markwick, A. J. 2024, *A&A*, 682, A109, doi: [10.1051/0004-6361/202346908](https://doi.org/10.1051/0004-6361/202346908)
- Müller, H. S. P., & Gerry, M. C. L. 1995, *J. Chem. Phys.*, 103, 577, doi: [10.1063/1.470092](https://doi.org/10.1063/1.470092)
- Müller, H. S. P., Schlöder, F., Stutzki, J., & Winniewisser, G. 2005, *Journal of Molecular Structure*, 742, 215, doi: [10.1016/j.molstruc.2005.01.027](https://doi.org/10.1016/j.molstruc.2005.01.027)

- Müller, H. S., & Brünken, S. 2005, *Journal of Molecular Spectroscopy*, 232, 213, doi: <https://doi.org/10.1016/j.jms.2005.04.010>
- Nava, M., Martin-Drumel, M.-A., Lopez, C. A., et al. 2016, *JACS*, 138, 11441, doi: [10.1021/jacs.6b05886](https://doi.org/10.1021/jacs.6b05886)
- Noah, M., Poetz, S., Vieth-Hillebrand, A., & Wilkes, H. 2015, *Environmental Science & Technology*, 49, 6466, doi: [10.1021/es506013m](https://doi.org/10.1021/es506013m)
- Peterson, K. A., & Dunning, Jr., T. H. 2002, *J. Chem. Phys.*, 117, 10548, doi: [10.1063/1.1520138](https://doi.org/10.1063/1.1520138)
- Pickett, H. M. 1991, *Journal of Molecular Spectroscopy*, 148, 371
- Pickett, H. M., Poynter, R. L., Cohen, E. A., et al. 1998, *Journal of Quantitative Spectroscopy and Radiative Transfer*, 60, 883
- Puskar, L., Robertson, E. G., & McNaughton, D. 2006, *J. Mol. Spectrosc.*, 240, 244, doi: [10.1016/j.jms.2006.10.001](https://doi.org/10.1016/j.jms.2006.10.001)
- Quénard, D., Jiménez-Serra, I., Viti, S., Holdship, J., & Coutens, A. 2018, *MNRAS*, 474, 2796, doi: [10.1093/mnras/stx2960](https://doi.org/10.1093/mnras/stx2960)
- Requena-Torres, M. A., Martín-Pintado, J., Martín, S., & Morris, M. R. 2008, *The ApJ*, 672, 352
- Requena-Torres, M. A., Martín-Pintado, J., Rodríguez-Franco, A., et al. 2006, *A&A*, 455, 971, doi: [10.1051/0004-6361:20065190](https://doi.org/10.1051/0004-6361:20065190)
- Rivilla, V. M., Martín-Pintado, J., Jiménez-Serra, I., et al. 2019, *MNRAS*, 483, L114
- . 2020, *ApJL*, 899, L28
- Rivilla, V. M., Jiménez-Serra, I., Martín-Pintado, J., et al. 2021a, *Proceedings of the National Academy of Science*, 118, 2101314118
- Rivilla, V. M., Jiménez-Serra, I., García de la Concepción, J., et al. 2021b, *MNRAS*, 506, L79
- Rivilla, V. M., Colzi, L., Jiménez-Serra, I., et al. 2022, *ApJL*, 929, L11
- Rivilla, V. M., García De La Concepción, J., Jiménez-Serra, I., et al. 2022b, *Frontiers in Astronomy and Space Sciences*, 9, 829288, doi: [10.3389/fspas.2022.829288](https://doi.org/10.3389/fspas.2022.829288)
- Rivilla, V. M., Jiménez-Serra, I., Martín-Pintado, J., et al. 2022c, *Frontiers in Astronomy and Space Sciences*, 9, doi: [10.3389/fspas.2022.876870](https://doi.org/10.3389/fspas.2022.876870)
- Rivilla, V. M., Sanz-Novato, M., Jiménez-Serra, I., et al. 2023, *ApJL*, 953, L20, doi: [10.3847/2041-8213/ace977](https://doi.org/10.3847/2041-8213/ace977)
- Rodríguez-Almeida, L. F., Jiménez-Serra, I., Rivilla, V. M., et al. 2021, *ApJL*, 912, L11
- Rodríguez-Fernández, N. J., Martín-Pintado, J., de Vicente, P., et al. 2000, *A&A*, 356, 695
- Sanz-Novato, M., Rivilla, V. M., Jiménez-Serra, I., et al. 2023, *ApJ*, 954, 3, doi: [10.3847/1538-4357/ace523](https://doi.org/10.3847/1538-4357/ace523)
- . 2024, arXiv e-prints, arXiv:2402.15405, <https://arxiv.org/abs/2402.15405>
- Shi, Q., Hou, D., Chung, K. H., et al. 2010, *Energy & Fuels*, 24, 2545, doi: [10.1021/ef901564e](https://doi.org/10.1021/ef901564e)
- Snyder, L. E., Hollis, J. M., Ulich, B. L., et al. 1975, *ApJ*, 198, L81
- Tercero, F., López-Pérez, J. A., Gallego, J. D., et al. 2021, *A&A*, 645, A37, doi: [10.1051/0004-6361/202038701](https://doi.org/10.1051/0004-6361/202038701)
- Tsuge, M., Molpeceres, G., Aikawa, Y., & Watanabe, N. 2023, *Nature Astronomy*, 7, 1351, doi: [10.1038/s41550-023-02071-0](https://doi.org/10.1038/s41550-023-02071-0)
- Vidal, T. H. G., Loison, J.-C., Jaziri, A. Y., et al. 2017, *MNRAS*, 469, 435, doi: [10.1093/mnras/stx828](https://doi.org/10.1093/mnras/stx828)
- Wilson, T. L., & Rood, R. 1994, *ARA&A*, 32, 191, doi: [10.1146/annurev.aa.32.090194.001203](https://doi.org/10.1146/annurev.aa.32.090194.001203)
- Wu, D., Hu, Q., & Zhu, D. 2018, *Oxidative Medicine and Cellular Longevity*, 2018, 4579140, doi: [10.1155/2018/4579140](https://doi.org/10.1155/2018/4579140)
- Yue, H. 2023, *Unravelling the Impacts of Palaeoecology, Palaeoenvironment and Lithofacies on Sedimentary Organic NSO Compounds (Doctoral Thesis, Technische Universität Berlin)*, doi: [10.14279/depositonce-18299](https://doi.org/10.14279/depositonce-18299)
- Zeng, S., Quénard, D., Jiménez-Serra, I., et al. 2019, *MNRAS*, 484, L43, doi: [10.1093/mnrasl/slz002](https://doi.org/10.1093/mnrasl/slz002)
- Zeng, S., Jiménez-Serra, I., Rivilla, V. M., et al. 2018, *MNRAS*, 478, 2962
- . 2021, *ApJL*, 920, L27
- Zeng, S., Rivilla, V. M., Jiménez-Serra, I., et al. 2023, *MNRAS*, 523, 1448, doi: [10.1093/mnras/stad1478](https://doi.org/10.1093/mnras/stad1478)
- Zhao, Y., Wang, Y., Xu, Q., et al. 2024, *Nitric Oxide*, 144, 29, doi: <https://doi.org/10.1016/j.niox.2024.01.003>
- Zheng, S., Li, J., Wang, J., et al. 2024, *ApJ*, 961, 58, doi: [10.3847/1538-4357/ad072c](https://doi.org/10.3847/1538-4357/ad072c)
- Ziegs, V., Noah, M., Poetz, S., et al. 2018, *Marine and Petroleum Geology*, 94, 114, doi: <https://doi.org/10.1016/j.marpetgeo.2018.03.039>

APPENDIX

A. SPECTROSCOPIC PROPERTIES AND PARAMETERS OF THIONYLIMIDE

The rotational spectrum of thionylimide, HNSO, was investigated by conventional microwave spectroscopy (Kirchhoff 1969; Borgo et al. 1979) with accuracies of 100 and 50 kHz, respectively. A Fourier transform microwave (FTMW) spectroscopy was capable of resolving not only the hyperfine structure (HFS) splitting of ^{14}N , but also that of ^1H (Heineking & Gerry 1993). The ground state rotational parameters were improved later through ground state combination differences (GSCDs) from a high-resolution infrared study (Joo et al. 1996).

We have fitted the available rotational data by applying the rotational and centrifugal distortion parameters from Joo et al. (1996) and the HFS parameters from Heineking & Gerry (1993). Moreover, the rotational spectrum calculated from the resulting spectroscopic parameters displayed fairly large uncertainties already for transitions with low quantum numbers. The underlying GSCDs from Joo et al. (1996) were unfortunately not available anymore from the corresponding author of that study. We received GSCDs from the authors of a different high-resolution infrared study (Puskar et al. 2006). Inclusion of essentially all of these GSCDs improved the uncertainties of the rotational and centrifugal distortion parameters greatly, permitted the sextic distortion parameters determined in the earlier infrared study and even the octic L_K to be fit as well. Only L_{KKJ} was very uncertain and was kept fixed to the value from the earlier study (Joo et al. 1996). Since the molecule is rather close to the prolate symmetric limit, it is advisable to employ Watson’s S reduction of the rotational Hamiltonian instead of the A reduction as used earlier. The change in reduction had the advantage that the parameter h_3 , which is the equivalent to ϕ_K in the A reduction, could be omitted in the present fit without significant deterioration of the quality of the fit.

The ^1H HFS splitting of 3.0 kHz observed in the $F_1 = 2 - 1$ component of the $J = 1 - 0$ a -type transition (Heineking & Gerry 1993) could not be explained by ^1H nuclear spin-rotation coupling, but required the ^1H - ^{14}N nuclear spin-nuclear spin coupling to be considered as well. This coupling is described by two terms of which the direct term can be calculated well from the geometry for light nuclei. Deviations are small even for moderately heavy nuclei, such as Cl, as are the contributions from the indirect term, but matter both for heavier nuclei, as shown for example in a study on BrF

and IF (Müller & Gerry 1995). The HN bond is almost perfectly aligned with the b -axis, and a value of $S_{bb} = -8.02$ kHz was derived from the structure. The ^1H and ^{14}N nuclear spin-rotation parameter $C_{ii}(\text{H})$ and $C_{ii}(\text{N})$ were necessary in the fit, but were not determined very accurately; the uncertainties were in part as large as the values, and in the most favorable cases smaller by only by a factor of a few. Therefore, we evaluated these parameters through quantum-chemical calculations employing the commercially available program Gaussian 16 (Frisch et al. 2019). We performed B3LYP hybrid density functional (Becke 1993; Lee et al. 1988) calculations using the aug-cc-pwCVTZ basis set (i.e., a valence basis set of triple zeta quality and augmented with diffuse basis functions Dunning, Jr. 1989 and with core-correlating basis functions Peterson & Dunning, Jr. 2002). Trial fits with these parameters kept fixed or with one to all released gave fits of essentially the same quality. Also, none of the parameters released in the fit changed its value significantly outside the respective parameters. Therefore, we kept the nuclear spin rotation parameters fixed at the quantum-chemically calculated values. The resulting spectroscopic parameters are given in Table A1 together with previous values (Joo et al. 1996; Heineking & Gerry 1993). The rotational spectrum calculated from these parameters is available in the catalog section of the CDMS (entry 63514). Its accuracy is sufficient for radio astronomical observations of cold objects, where molecules show low T_{ex} (i.e., 10–20 K), including prestellar cores and also the G+0.693 molecular cloud, and probably also for a warm source with $T_{\text{ex}} \lesssim 80$ K. However, this catalogue may not be accurate enough for, e.g., hot cores or hot corinos with $T_{\text{ex}} \gtrsim 100$ K. The underlying line, parameter, and fit files along with other auxiliary files are available in the catalog archive of the CDMS (Müller et al. 2005; Endres et al. 2016).

The agreement of the rotational and centrifugal distortion parameters from this study and from Joo et al. (1996) is, unsurprisingly, good when the change in reduced Hamiltonian is taken into account. The diagonal quartic distortion parameters D_J , D_{JK} , and D_K differ from the corresponding Δ_J , Δ_{JK} , and Δ_K by small multiples of d_2 ; $\delta_J = -d_1$, and only the relation between d_2 and δ_K are somewhat more complex. The differences in values are mostly caused by the change in reduction. Similar, albeit more complex relations apply to the sextic distortion parameter to convert from one reduction

Table A1. Present and previous spectroscopic parameters^a (MHz) of thionylimide.

Parameter	Present	Previous	Parameter
A	49315.8592 (84)	49315.8695 (36)	A
B	9869.75936 (23)	9869.80628 (24)	B
C	8205.14749 (23)	8205.10205 (24)	C
D_K	1.46953 (29)	1.47025 (3)	Δ_K
$D_{JK} \times 10^3$	-89.408 (41)	-90.746 (8)	$\Delta_{JK} \times 10^3$
$D_J \times 10^3$	6.6754 (21)	6.9107 (6)	$\Delta_J \times 10^3$
$d_1 \times 10^3$	-1.9211 (10)	1.9227 (2)	$\delta_J \times 10^3$
$d_2 \times 10^3$	-0.11925 (42)	23.122 (16)	$\delta_K \times 10^3$
$H_K \times 10^6$	143.2 (11)	143.5 (1)	$\Phi_K \times 10^6$
$H_{KJ} \times 10^6$	-9.20 (11)	-10.42 (7)	$\Phi_{KJ} \times 10^6$
$H_{JK} \times 10^6$	-0.317 (18)	0.055 (20)	$\Phi_{JK} \times 10^6$
$H_J \times 10^9$	11.92 (67)	12.49 (13)	$\Phi_J \times 10^9$
$h_1 \times 10^9$	5.86 (38)	6.72 (8)	$\phi_J \times 10^9$
$h_3 \times 10^9$	-	12.1 (6)	$\phi_K \times 10^6$
$L_K \times 10^9$	-16.0 (11)	-15.90 (7)	$L_K \times 10^9$
$L_{KKJ} \times 10^9$	1.1	1.10 (4)	$L_{KKJ} \times 10^9$
χ_{aa}	-1.5757 (16)	-1.5756 (29)	χ_{aa}
χ_{bb}	-0.0250 (14)	-0.0255 (24) ^b	χ_{bb}
χ_{cc}	1.6007 (14) ^b	1.6011 (24) ^b	χ_{cc}
$C_{aa}(\text{N}) \times 10^3$	9.38	-	$C_{aa}(\text{N}) \times 10^3$
$C_{bb}(\text{N}) \times 10^3$	2.60	2.3 (15) ^b	$C_{bb}(\text{N}) \times 10^3$
$C_{cc}(\text{N}) \times 10^3$	0.65	0.8 (15) ^b	$C_{cc}(\text{N}) \times 10^3$
$C_{aa}(\text{H}) \times 10^3$	-4.44	-	$C_{aa}(\text{H}) \times 10^3$
$C_{bb}(\text{H}) \times 10^3$	1.62	1.9 (35) ^b	$C_{bb}(\text{H}) \times 10^3$
$C_{cc}(\text{H}) \times 10^3$	-1.10	-1.1 (35) ^b	$C_{cc}(\text{H}) \times 10^3$
$S_{bb} \times 10^3$	-8.02	-	$S_{bb} \times 10^3$

NOTE—^a Watson’s S reduction in the I^r representation was used in the present fit whereas Watson’s A reduction was used in the previous fit (Joo & Clouthier 1996). Hyperfine parameters were taken from Heineking & Gerry (1993). Numbers in parentheses are one standard deviation in units of the least significant figures. Numbers without uncertainties were kept fixed in the fit, see Section A. ^b Derived parameter. Heineking & Gerry (1993) determined χ_{aa} and $\chi_{bb} - \chi_{bb}$ for ¹⁴N and $C_{bb} + C_{cc}/2$ as well as $C_{bb} - C_{cc}$ for both nuclei.

to the other. Even though our fit contains one distortion parameter less than the fit in Joo et al. (1996), most of their uncertainties are smaller by factors of a few, suggesting their unavailable data set was more extensive or more accurate than the one available to us from Puskar et al. (2006). The uncertainties of B and C are essentially the same, which is most likely a consequence of a too low weight of the two hyperfine free transition frequencies of Heineking & Gerry (1993) in the fit of Joo et al. (1996). The present nuclear quadrupole coupling parameters agree well with those from Heineking & Gerry (1993); this applies also to the nuclear spin-rotation parameters if we take the relatively large uncertainties from the previous study into account.

Finally, we provide in Table A2 the rotational (Q_r) partition function of the ground state of HNSO. We used SPCAT (Pickett 1991) to estimate the values of Q_r by

direct summation of the ground state energy levels up to $J = 125$ and $K_a = 62$. These values are provided for the conventional temperatures as implemented in the JPL database (Pickett et al. 1998), and two additional temperatures of 2.725 K and 5.000 K.

B. ANALYSIS OF NS

For completeness, we also present the LTE analysis of NS ($^2\Pi_{1/2}$ state), which was performed using all the most unblended transitions (see Table B1). We obtained the spectroscopic data from the 046515 entry of the CDMS catalogue (Lee et al. 1995). We present in Figure B1 the result of the best LTE fit using the AUTOFIT tool within SLIM. As shown, the hyperfine structure of NS is partially resolved within the astronomical data set. We derived the following physical parameters from the fit: $N = (28 \pm 3) \times 10^{13} \text{ cm}^{-2}$, $T_{\text{ex}} = (7.5 \pm 0.5) \text{ K}$,

Table A2. Rotational (Q_r) partition function of HNSO.

Temperature (K)	Q_r
2.725	37.8087
5.000	91.8833
9.375	233.001
18.75	654.456
37.50	1844.94
75.00	5211.15
150.0	14737.8
225.0	27087.7
300.0	41729.9

$v_{\text{LSR}} = (70.6 \pm 0.6) \text{ km s}^{-1}$ and $\text{FWHM} = (19 \pm 1) \text{ km s}^{-1}$. The derived column density is translated into a fractional abundance with respect to H_2 of $(2.1 \pm 0.2) \times 10^{-9}$. In Figure B1, we depict the fitted line profiles of NS in red, while the expected molecular emission from all the molecules detected to date toward G+0.693 is shown in blue.

C. ANALYSIS OF SO_2

We carried out the LTE analysis for SO_2 by using the most intense and unblended transitions clearly detected toward G+0.693 (see Table C1). The spectroscopic data were acquired from the 064502 entry of the CDMS catalogue (Müller & Brünken 2005). In Figure C1 we show the result of the best LTE fit derived from AUTOFIT. We obtained the following physical parameters from the LTE fit: $N = (38.4 \pm 0.5) \times 10^{13} \text{ cm}^{-2}$, $T_{\text{ex}} = (18.9 \pm 0.2) \text{ K}$, $v_{\text{LSR}} = (68.9 \pm 0.1) \text{ km s}^{-1}$ and $\text{FWHM} = (21.1 \pm 0.3) \text{ km s}^{-1}$. Thus, we derived a fractional abundance with respect to molecular hydrogen of $(2.8 \pm 0.3) \times 10^{-9}$. We used the same color code for the line profiles of Figure C1 as that of Fig. 1 (i.e., fitted line profiles of SO_2 in red and the expected molecular emission from all the molecules detected to date toward G+0.693 in blue).

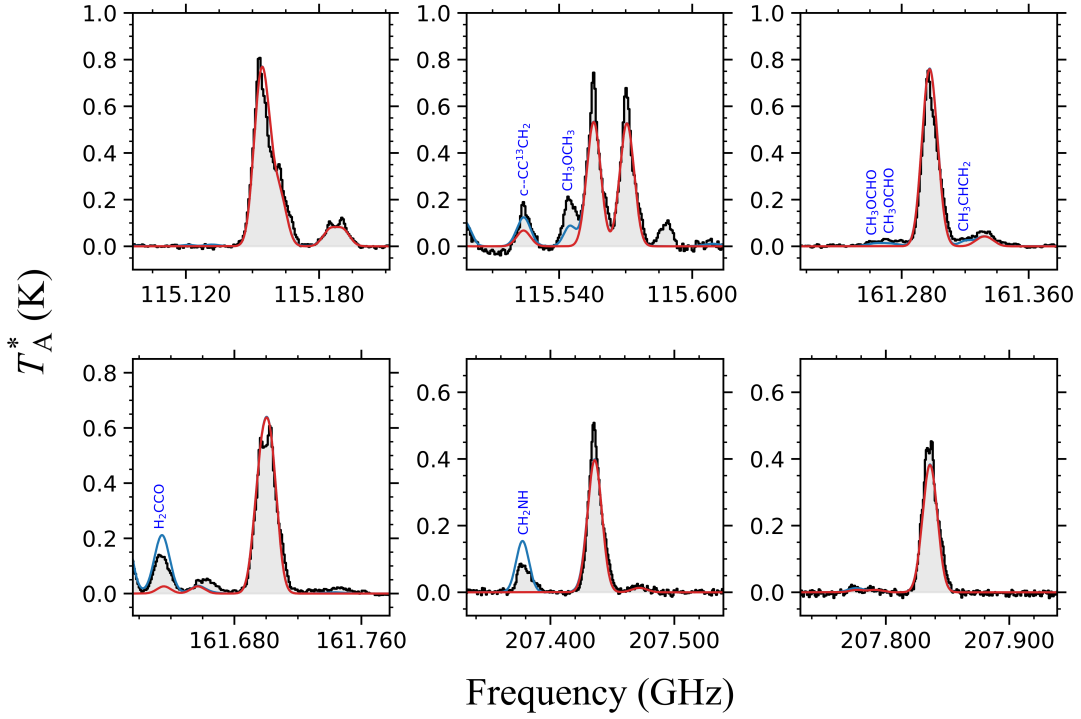


Figure B1. Unblended or slightly blended transitions of NS detected toward G+0.693 molecular cloud (listed in Table C1). The result of the best LTE fit is shown with a red solid line, while the blue line shows the expected molecular emission from all the molecular species identified to date in our survey. The observed spectra are plotted as gray histograms.

Table B1. Spectroscopic information of the unblended transitions of NS^(a) detected toward G+0.693 (shown in Figure B1).

Parity	Frequency (GHz)	$J' - J''$	$F' - F''$	$\log I$ (300 K) (nm ² MHz)	g_u	E_{up} (K)	rms (mK)	$\int T_A^* dv$ (mK km s ⁻¹)	S/N ^(b)	Blending
e	115.153935 (20)	2.5 - 1.5	3.5 - 2.5	-3.3836	8	8.8	9.1	22190	425	Unblended
e	115.156812 (20)	2.5 - 1.5	2.5 - 1.5	-3.5843	6	8.8				Unblended
e	115.162982 (20)	2.5 - 1.5	1.5 - 0.5	-3.3836	4	8.8				Unblended
e	115.185336 (9)	2.5 - 1.5	1.5 - 1.5	-3.3836	4	8.8	9.1	3189	61	Unblended
e	115.191456 (12)	2.5 - 1.5	2.5 - 2.5	-3.3836	6	8.8				Unblended
f	115.524603 (20)	2.5 - 1.5	1.5 - 1.5	-4.3015	4	8.8	9.1	2067	50	c-CC ¹³ CH ₂
f	115.556253 (20)	2.5 - 1.5	3.5 - 2.5	-3.3807	8	8.8	9.1	13159	252	Unblended
f	115.570763 (20)	2.5 - 1.5	2.5 - 1.5	-3.5814	6	8.8	9.1	12290	236	Unblended
f	115.571954 (20)	2.5 - 1.5	1.5 - 0.5	-3.8067	4	8.8				Unblended
e	161.297246 (20)	3.5 - 2.5	4.5 - 3.5	-2.9737	10	16.5	2.0	16153	1409	Unblended
e	161.298411 (20)	3.5 - 2.5	3.5 - 2.5	-3.1076	8	16.5				Unblended
e	161.301747 (20)	3.5 - 2.5	2.5 - 1.5	-3.2467	6	16.5	2.0	2281	199	CH ₃ CHCH ₂
e	161.330290 (10)	3.5 - 2.5	2.5 - 2.5	-4.1587	6	16.5				Unblended
f	161.636517 (20)	3.5 - 2.5	3.5 - 3.5	-4.1567	8	16.5	2.0	3150	275	H ₂ CCO
f	161.657816 (20)	3.5 - 2.5	2.5 - 2.5	-4.1567	6	16.5	2.0	1104	96	Unblended
f	161.697257 (20)	3.5 - 2.5	4.5 - 3.5	-2.9717	10	16.5	2.0	16860	1471	Unblended
f	161.703404 (20)	3.5 - 2.5	3.5 - 2.5	-3.1055	8	16.5				Unblended
f	161.703987 (20)	3.5 - 2.5	2.5 - 1.5	-3.2446	6	16.5				Unblended
e	207.436051 (6)	5.5 - 4.5	5.5 - 4.5	-2.6730	12	26.4	7.5	9050	211	Unblended
e	207.436636 (5)	5.5 - 4.5	4.5 - 3.5	-2.7742	10	26.4				Unblended
e	207.438692 (20)	5.5 - 4.5	3.5 - 2.5	-2.8771	8	26.4				Unblended
e	207.470606 (11)	5.5 - 4.5	3.5 - 3.5	-4.0586	8	26.4	7.5	282	7	Unblended
e	207.475341 (11)	5.5 - 4.5	4.5 - 4.5	-4.0586	10	26.4				Unblended
f	207.834866 (20)	5.5 - 4.5	5.5 - 4.5	-2.6715	12	26.4	7.5	9511	221	Unblended
f	207.838365 (20)	5.5 - 4.5	4.5 - 3.5	-2.7727	10	26.4				Unblended
f	207.838365 (20)	5.5 - 4.5	3.5 - 2.5	-2.8756	8	26.4				Unblended

NOTE—^(a) The rotational energy levels are labelled using the quantum number J and F . The parity is also indicated. For those hyperfine components that are partially or fully coalesced, we provide the integrated intensity and S/N ratio of the mean observed line rather than the values of each component, which is given only once for each group of transitions. Numbers in parentheses represent the predicted uncertainty associated to the last digits.

Table C1. Spectroscopic information of the selected transitions of SO₂ detected toward G+0.693 (shown in Figure C1).

Frequency (GHz)	Transition ^(a)	log <i>I</i> (300 K) (nm ² MHz)	<i>g</i> _u	<i>E</i> _{up} (K)	rms (mK)	$\int T_{\Lambda}^* dv$ (mK km s ⁻¹)	S/N ^(b)	Blending
83.6880930 (20)	8 _{1,7} -8 _{0,8}	-3.9576	17	36.5	1.3	4778	641	Unblended
104.0294183 (20)	3 _{1,3} -2 _{0,2}	-4.2264	7	2.7	1.2	9547	1388	Unblended
104.2392952 (20)	10 _{1,9} -10 _{0,10}	-3.7708	21	54.3	1.2	2619	381	Unblended
131.014860 (80)	12 _{1,11} -12 _{0,12}	-3.6063	25	75.9	5.4	831	27	CH ₃ NC
135.696020 (80)	5 _{1,5} -4 _{0,4}	-3.8143	11	15.6	1.6	12587	1373	Unblended
160.827880 (80)	10 _{0,10} -9 _{1,9}	-3.4028	21	49.4	2.1	7239	602	CH ₃ OCH ₃
163.6055328 (6)	14 _{1,13} -14 _{0,14}	-3.4644	29	101.0	1.6	430	47	Unblended
165.2254511 (8)	7 _{1,7} -6 _{0,6}	-3.5083	15	26.9	1.6	9703	1058	Unblended
203.39155 (10)	12 _{0,12} -11 _{1,11}	-3.1094	25	69.6	9.3	3668	69	Unblended

NOTE—^(a) The rotational energy levels are labelled using the conventional notation for asymmetric tops: J_{K_a, K_c} , where J denotes the angular momentum quantum number, and the K_a and K_c labels are projections of J along the a and c principal axes. Numbers in parentheses represent the predicted uncertainty associated to the last digits.

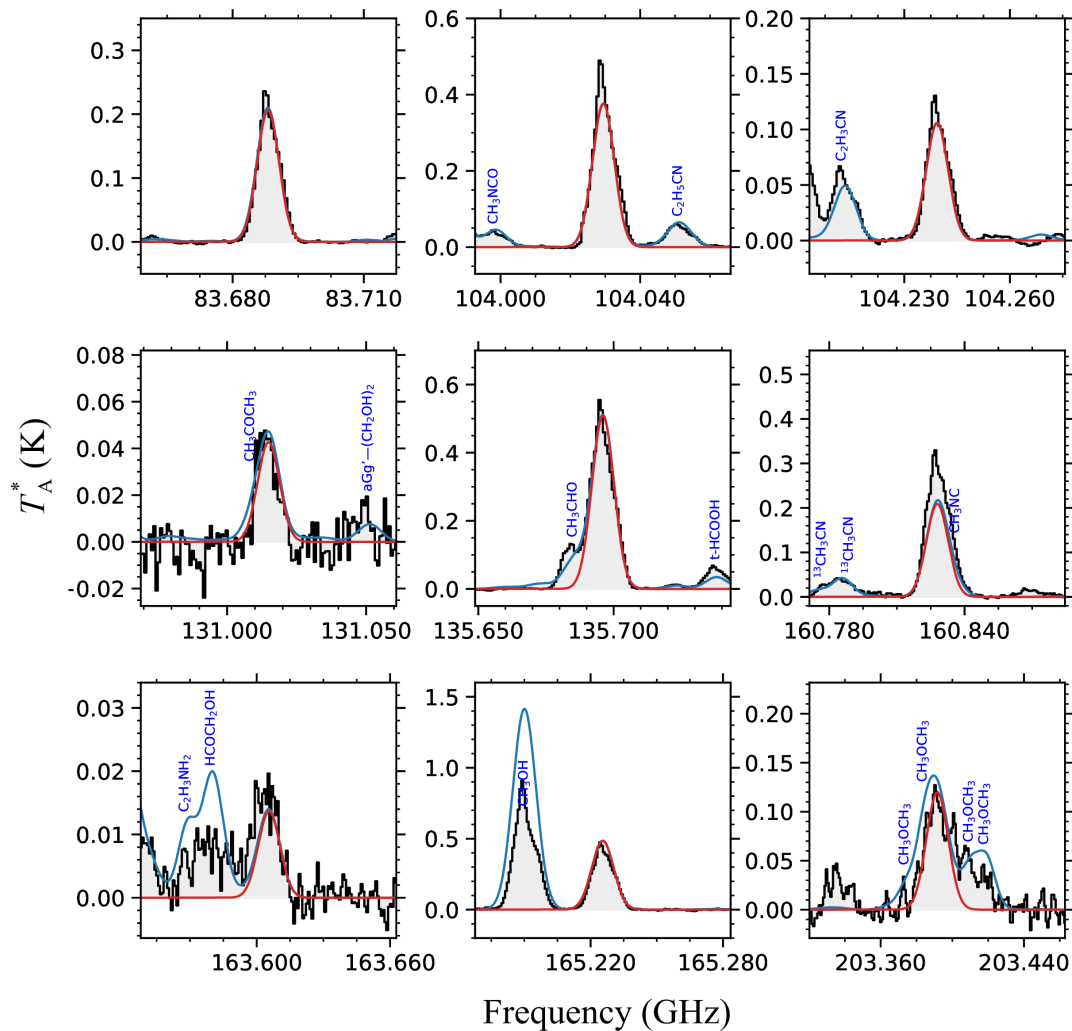


Figure C1. Unblended or slightly blended transitions of SO_2 detected toward G+0.693 molecular cloud (listed in Table C1). The result of the best LTE fit is shown with a red solid line, while the blue line shows the expected molecular emission from all the molecular species identified to date in our survey. The observed spectra are plotted as gray histograms.